Applied Catalysis B: Environmental 147 (2014) 726–732

Contents lists available at ScienceDirect

Applied Catalysis B: Environmental

journal homepage: www.elsevier.com/locate/apcatb

Hydrothermally sulfonated single-walled carbon nanohorns for use as solid catalysts in biodiesel production by esterification of palmitic acid

Chantamanee Poonjarernsilp[a,b,*], Noriaki Sano[a], Hajime Tamon[a]

[a] Department of Chemical Engineering, Graduate School of Engineering, Kyoto University, Nishikyo-ku, Kyoto 615-8510, Japan
[b] Department of Chemical Engineering, Faculty of Engineering, Rajamangala University of Technology Krungthep, Sathorn, Bangkok 10120, Thailand

ARTICLE INFO

Article history:
Received 3 June 2013
Received in revised form 6 September 2013
Accepted 8 October 2013
Available online 16 October 2013

Keywords:
Single-walled carbon nanohorns
Solid acid catalyst
Sulfonation
Esterification
Biodiesel

ABSTRACT

Four carbon-based solid acid catalysts were prepared from single-walled carbon nanohorns (SWCNHs), oxidized SWCNHs (ox-SWCNHs), activated carbon (AC), and carbon black (CB) by hydrothermal sulfonation at 200 °C in an autoclave reactor. N_2 adsorption analysis suggested that sulfonation treatment leads to a drastic reduction in the number of relatively large pores with diameters greater than 20 nm in the SWCNHs and ox-SWCNHs. In addition, the BET surface area of the SWCNH was doubled by this sulfonation. These structural changes were not observed in AC and CB. The acid functional group formed on these solid catalysts by sulfonation was speculated to be $-SO_3H$, and this was analyzed by ion-exchange titration. From the results, it was found that sulfonated SWCNHs (SO_3H-SWCNHs) had the highest acid density of the four sulfonated specimens, which is a desirable property for its use as a biodiesel production catalyst. Methyl palmitate, a kind of biodiesel, was produced by the esterification of palmitic acid using these four catalysts. SO_3H-SWCNHs produced the highest yield and the catalytic activity was significantly higher than that using a homogeneous sulfuric acid catalyst. Repeated esterification experiments suggested that the acid sites on SO_3H-SWCNHs and SO_3H-ox-SWCNHs were more stable than those on SO_3H-AC and SO_3H-CB.

1. Introduction

Biodiesel is an environmentally sustainable fuel composed of alkyl esters of long-chain fatty acids. It can be made from vegetable oils, animal fat, and waste oils from the food industry [1–5]. In general, biodiesel is produced by the catalytic esterification of free fatty acids (FFAs) or catalytic transesterification of triglyceride with alcohols [5,6]. The conventional catalysts for these reactions are homogeneous strong bases or acids such as sodium hydroxide or sulfuric acid, respectively [7]. These catalysts are highly efficient and have low costs. However, when the raw materials such as palm oil or waste oil contain a high percentage of FFA, the alkali catalyst reacts with the FFAs to form soaps. This reaction, which is called saponification, not only consumes the catalyst, but also reduces the yield of the biodiesel product [8]. In this situation, an acid catalyst is preferable because it can inhibit the saponification reaction. However, homogeneous acid catalysts also have several drawbacks such as equipment corrosion, difficulty of handling, and problems separating the products from the catalysts. For these reasons, the development of heterogeneous solid acid catalysts is desirable, and many types of solid-acid catalysts have been developed to activate the esterification of low-cost feedstocks such as waste cooking oil in order to achieve efficient and low-cost biodiesel production.

It has been reported that sulfonated ion-exchange resin [9,10], zeolite [11], heteropolyacid [12], and sulfated zirconia [13,14] can be used as such heterogeneous acid catalysts. However, catalysts with micropores, such as zeolites, are not suitable for biodiesel production because the micropores limit the diffusion of large molecules with long alkyl chains [15,16]. Ion-exchange resins are active strong acids, but they have a low thermal stability and deactivation occurs after only 2–5 h [17,18]. In the case of sulfated zirconia, the catalyst stability is reduced by the blocking of the small pores by larger product molecules and coke formation [15,19].

Other than these solid acid catalysts, a new class of sulfonated carbon-based solid acid catalyst has been reported as being a promising catalyst for biodiesel production [5,20–27], especially for the esterification of FFA. Carbon-based solid acid catalysts are superior for their high mechanical and thermal stabilities, which should help to maintain their unique mesoporous properties. In addition, the hydrophobic property of their surface is an important feature of these carbon materials, as it attracts the organic reactants and retards unfavorable reactions caused by the presence of H_2O. However, reports of using carbon-based solid acid catalysts to produce biodiesel by esterification of FFA are still rare, and thus, the

* Corresponding author at: Department of Chemical Engineering, Graduate School of Engineering, Kyoto University, Nishikyo-ku, Kyoto 615-8510, Japan.
Tel.: +81 75 383 2684; fax: +81 75 383 2684.
E-mail address: chantamanee.w@rmutk.ac.th (C. Poonjarernsilp).

0926-3373/$ – see front matter © 2013 Elsevier B.V. All rights reserved.
http://dx.doi.org/10.1016/j.apcatb.2013.10.006

investigation of these materials, especially nanotube-type materials [25], is very important.

One of the candidates among such materials is the single-walled carbon nanohorn (SWCNH). As SWCNHs have a high surface area, chemical resistance, thermal stability, and are hydrophobic [28–32], they can be used in many applications such as catalyst supports for fuel cells [32,33], gas storage [31,34], and drug carriers [35]. In the present study, the superior performance of SWCNHs for use as a catalyst for biodiesel production is reported for the first time.

In this study, a hydrothermal method using sulfuric acid was employed to sulfonate SWCNHs to prepare solid acid catalysts, and the reactivity of these catalysts were evaluated with respect to their performance in catalyzing the esterification reaction to generate a biodiesel. The influence of oxidation pretreatment on the SWCNH was assessed. For comparison, activated carbon (AC) and carbon black (CB) were also sulfonated. For an additional comparison, a sulfuric acid solution was used as a representative conventional homogeneous acid catalyst.

2. Experimental

2.1. Materials

To synthesize the SWCNHs, a method using an arc discharge in water with nitrogen gas injection was employed [36,37]. To generate the arc discharge, a graphite rod anode (purity 99.99%, 6 mm in diameter) was shifted toward the cathode (20 mm in diameter) along its vertical axis. A hole (12 mm in diameter and 25 mm in length) was drilled in the bottom of the cathode such that the arc discharge was generated these electrodes in the cathode hole. Both electrodes were submerged in water to cool the carbon vapor emitted from the arc discharge zone. The carbon vapor was expelled by an N_2 flow (10 L/min) introduced from four narrow channels (3 mm in diameter) located on the top of the cathode to enhance cooling. The arc discharge was generated by supplying DC current at 80 A. Using these conditions, as-grown SWCNH was synthesized during the 1-min duration of the arc discharge, and then the floating powdery products were collected from the water surface.

To increase the surface area of the SWCNH, the as-grown product was mildly oxidized by heating in air with an electric furnace at 500 °C for 30 min. After this oxidation, the weight loss of the SWCNH was determined to be 23%. Hereinafter, the oxidized SWCNH is referred to as ox-SWCNH.

AC generated from charcoal was used to prepare a catalyst for comparison with SWCNH. CB (Aldrich, 99.95%, mesoporous) was purchased from Sigma–Aldrich.

For the sulfonation treatment of these carbonaceous materials and the biodiesel production experiments, sulfuric acid (H_2SO_4, 95%), methanol (CH_4O, 99.8%), palmitic acid ($C_{16}H_{32}O_2$, 95%), methyl palmitate ($C_{17}H_{34}O_2$, 98%), sodium chloride (NaCl, 99.5%), and 0.01 mol/L sodium hydroxide (NaOH, factor = 0.98) were purchased from Wako Chemical, Inc.

2.2. Catalyst preparation by hydrothermal sulfonation

Four types of carbonaceous materials (SWCNH, ox-SWCNH, AC, and CB) were sulfonated to prepare the solid acid catalysts. In this sulfonation process, 1 g of the carbon sample was immersed in 20 mL of sulfuric acid (95%) in a 100-mL Teflon autoclave, and then it was heated at 200 °C for 18 h. After this hydrothermal treatment, the obtained products were washed with distilled water at 80 °C on a membrane filter until the filtrate water became neutral in order to remove the remaining sulfuric acid, and then, they were dried at 90 °C for 24 h. These sulfonated catalysts were labeled as SO_3H-SWCH, SO_3H-ox-SWCNH, SO_3-AC, and SO_3H-CB.

2.3. Characterizations

2.3.1. Microscopic observation and crystallinity analysis

The morphologies of the sulfonated carbon-based catalysts were characterized by transmission electron microscopy (TEM) (JEOL, JEM-1010) at an accelerating voltage of 100 kV and field emission scanning electron microscopy (SEM) (JEOL, JSM-6700F). The crystallinity of these catalysts was evaluated by Raman spectroscopy (Lamda Vision Ltd., MicroRAM-300L) in the wave number range of 1000–2000 cm^{-1}.

2.3.2. BET surface area and pore structures

The surface areas of the catalysts were determined by the BET equation using N_2 adsorption isotherm with an automatic analyzer (Bel Japan, BELSORP-miniII-S). The pore volume was obtained from the amount of N_2 adsorbed, and the pore size distribution was calculated by the Barrett–Joyner–Halenda (BJH) method [38]. All samples were degassed at 200 °C for 2 h before the measurement.

2.3.3. Acid site density

To quantify the density of acid functional groups on the surface of the catalysts, the acid site density was estimated by ion-exchange titration [43]. In the first step of this titration, H^+ on the acid functional groups were exchanged with Na^+ by immersing 0.05 g of the catalyst in 10 mL of 2 mol/L NaCl solution at room temperature for 24 h under stirring (150 rpm). The H^+ concentration in the supernatant solution was expected to have equilibrated after this long contact time, and the solution was then titrated with 0.01 mol/L NaOH. Phenolphthalein was used to detect neutralization. The acid site density was calculated by the number of moles of NaOH titrated divided by the weight of the catalyst.

2.4. Evaluation of the catalytic activity

2.4.1. Esterification of palmitic acid

Liquid-phase esterification of palmitic acid with methanol was performed in a three-neck round-bottom flask (50 mL) connected to a water-cooled condenser. The reaction scheme is described by Eq. (1).

$$C_{16}H_{32}O_2 + CH_3OH \rightarrow C_{17}H_{34}O_2 + H_2O \quad (1)$$

The flask used for this reaction was placed in an oil bath placed on a magnetic stirring heater to maintain the reaction temperature at 64 °C. The catalysts were dried for 1 h at 100 °C in an oven before the catalytic tests. This esterification was performed by the following procedure: 0.15 g of palmitic acid was introduced into the flask, and then the temperature was increased to 64 °C. After the palmitic acid had melted, 5 g of warm methanol and 0.15 g of catalyst were quickly added and stirred rapidly by a magnetic bar at 600 rpm. (The weight ratio of palmitic acid to methanol was 1:33, and the concentration of the catalyst in the reaction solution was 3 wt%.) The temperature of this liquid-phase esterification reaction was kept at 64 °C for 5 h. Sample solutions were collected periodically from the flask during the reaction, and the concentration of the produced methyl palmitate was analyzed using a gas chromatograph (Shimadzu, GC-14B) equipped with a flame ionization detector and an adsorption column (GL Science Ltd., Unisole 3000, 3 mm in diameter and 2 m in length). Ar was used as the carrier gas. To compare the performance of the solid acid catalysts prepared in this study, sulfuric acid (0.15 g) was used as a homogeneous liquid catalyst.

The performance of the catalysts was evaluated by the yield of methyl palmitate, Y [%], and reaction turnover frequencies, TOF [min^{-1}]. Y is defined as the mole percentage of methyl palmitate

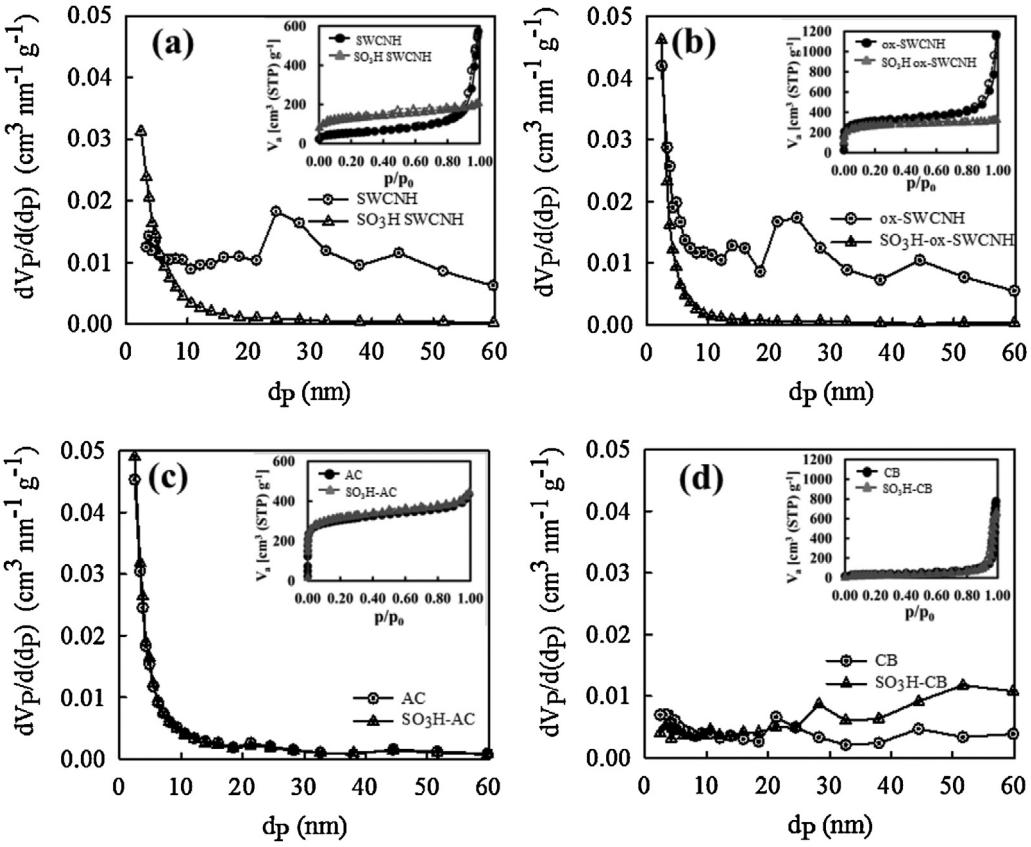

Fig. 1. Pore-size distribution of (a) SWCNH and SO_3H-SWCNH, (b) ox-SWCNH and SO_3H-ox-SWCNH, (c) AC and SO_3H-AC, and (d) CB and SO_3H-CB.

produced from reaction to methyl palmitate theoretically expected assuming perfect selectivity. TOF is evaluated in terms of palmitic acid ($C_{16}H_{32}O_2$) conversion to methyl palmitate ($C_{17}H_{34}O_2$) per number of moles of the acid site. From Eq. (1), one mole of methyl palmitate formation is produced from one mole of palmitic acid conversion. Thus in this study, TOFs for esterification reaction of palmitic acid were calculated from the reaction rate of methyl palmitate formation under initial rate of reaction within 2 h. TOFs is defined by Eq. (2) for each sulfonated solid catalyst.

$$\mathrm{TOF} = \frac{M_D}{\tau M_{CAT}} \quad (2)$$

where M_D is the number of moles of methyl palmitate produced in the reaction time, τ, and M_{CAT} is the number of moles of the acid site determined by ion-exchange titration. In this study, a reaction time of 2 h was used to determine TOF.

2.4.2. Catalyst reusability

To evaluate the reusability of the sulfonated solid catalysts, the esterification of palmitic acid was repeated three times. After each batch of the reaction, the catalyst was separated by filtration from the solution, and dried at room temperature. The dried catalyst was then reused for the next batch. For each batch, a fresh solution containing palmitic acid and methanol at the same concentrations as in the first batch was prepared.

3. Results and discussion

3.1. Pore structure and microscopic observation

To study the effects of sulfonation on the structures of the solid catalysts, their morphological features were investigated from the viewpoints of their pore structure and microscopic observation. Fig. 1 shows the pore-size distribution of the eight specimens: SWCNH, SO_3H-SWCNH, ox-SWCNH, SO_3H-ox-SWCNH, AC, SO_3H-AC, CB, and SO_3H-CB. The adsorption and desorption isotherm, from which the pore-size distributions were obtained, are inset in this figure. The BET surface area, obtained from N_2 adsorption, mesopore surface area, and mesopore volume measured for these specimens are summarized in Table 1.

It is remarkable that the pore-size distributions of SWCNH and ox-SWCNH changed drastically upon sulfonation, as shown in Fig. 1(a) and (b). In both cases, it is obvious that the number of relatively large pores with diameters greater than 20 nm decreased to a negligible level. In the case of SWCNH, the number of pores with diameters less than 10 nm significantly increased. Looking at the data in Table 1, it is noteworthy that the BET surface area of SWCNH doubled upon sulfonation from 210 cm^3/g to 418 cm^3/g, and this increase was due to the increase in the number of such small pores. Ox-SWCNH had a large surface area of 1002 cm^3/g, which was a result of micropores on SWCNH being opened by the mild oxidation treatment, whereas its surface area was not increased by

Table 1
BET surface area (S_{BET}), mesopore surface area (S_{meso}), and mesopore volume estimated using the BJH method (V_{meso}) of the various carbon-based solid catalysts.

Catalysts	S_{BET} ($m^2\,g^{-1}$)	S_{meso} ($m^2\,g^{-1}$)	V_{meso} (cm^3/g)
SWCNH	210	172	1.05
ox-SWCNH	1002	280	1.39
AC	948	183	0.27
CB	106	96	1.14
SO_3H-SWCNH	418	137	0.18
SO_3H-ox-SWCNH	855	149	0.15
SO_3H-AC	977	192	0.27
SO_3H-CB	104	100	0.99

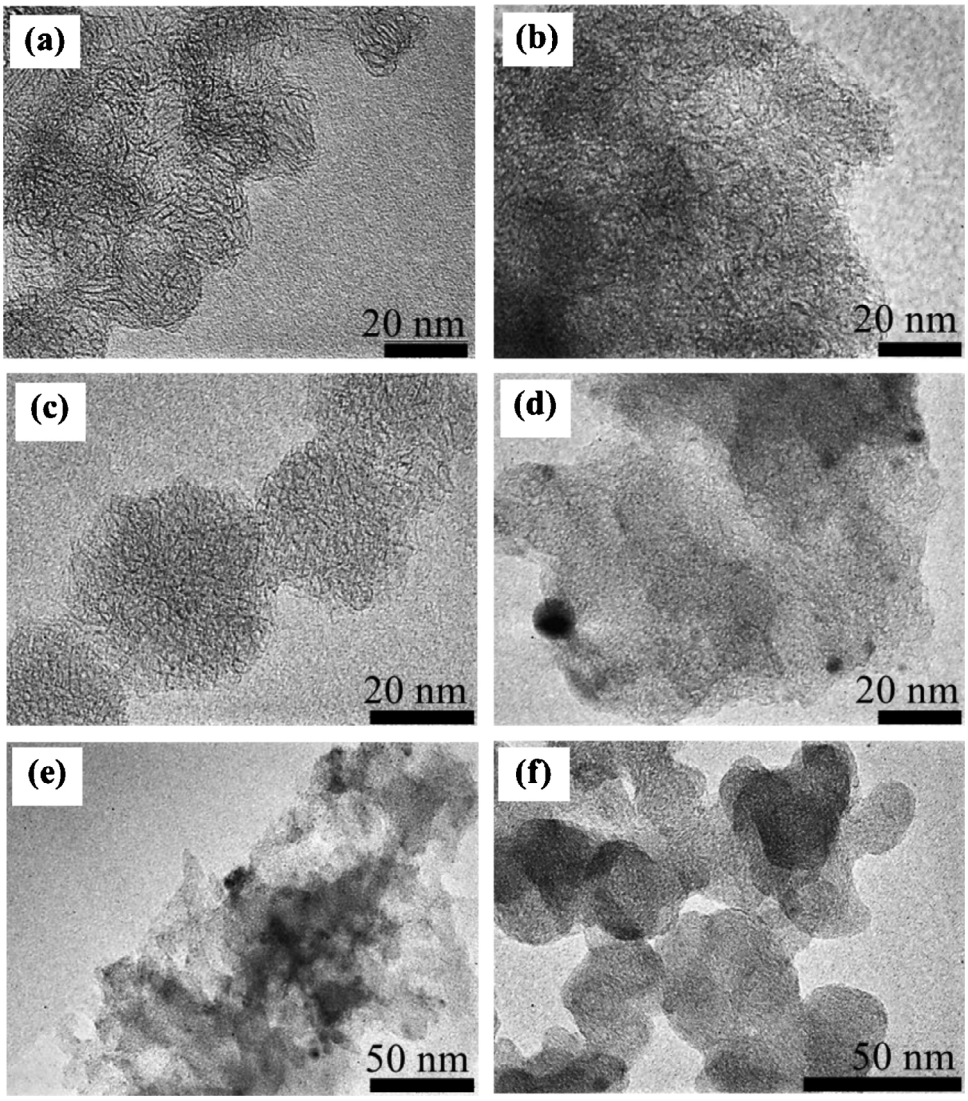

Fig. 2. TEM images of (a) SWCNH, (b) SO_3H-SWCNH, (c) ox-SWCNH, (d) SO_3H-ox-SWCNH, (e) SO_3H-AC, and (f) SO_3H-CB.

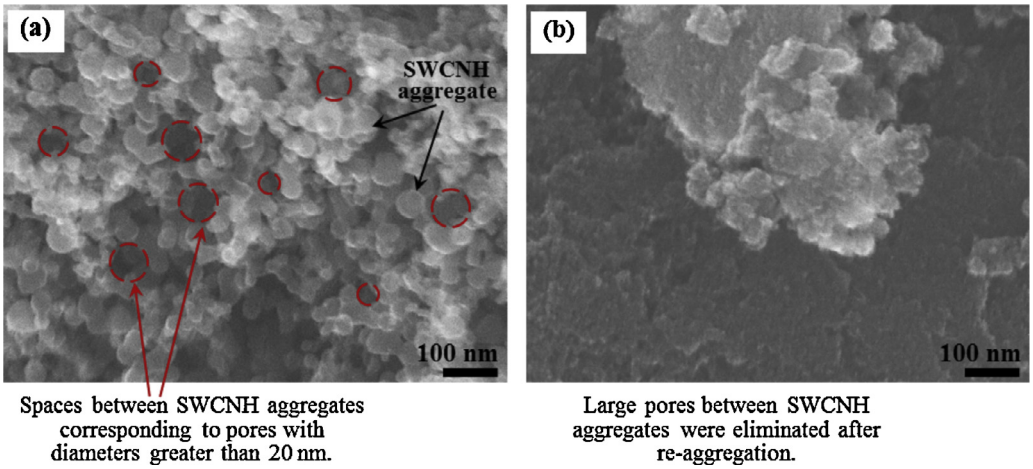

Fig. 3. SEM images of (a) as-grown SWCNHs and (b) SO_3H-SWCNHs showing the disappearance of pores with diameters greater than 20 nm through a re-aggregation mechanism.

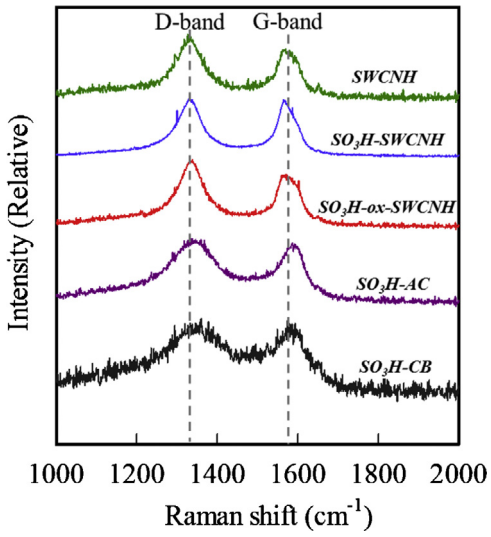

Fig. 4. Raman spectra of SWCNH, SO_3H-SWCNH, SO_3H-ox-SWCNH, SO_3H-AC, and SO_3H-CB.

sulfonation. Instead, its surface area decreased to 855 cm^3/g upon sulfonation owing to the partial destruction of its structure. In Table 1, the mesopore volume of SWCNH and ox-SWCNH were reduced by one order of magnitude upon sulfonation.

In spite of such changes to the pore structures of SWCNH and ox-SWCNH, the change in their structures by sulfonation was not so clear in the TEM observations. TEM images of SWCNH, SO_3H-SWCNH, ox-SWCNH, and SO_3H-ox-SWCNH are shown in Fig. 2(a)–(d). Nevertheless, it could be deduced by close observation that the aggregation of horns in SWCNH and ox-SWCNH after sulfonation seemed more prominent than before.

An explanation for the abovementioned change in the pore structures of SWCNH and ox-SWCNH could be as follows. (1) The relatively large pores with diameters greater than 20 nm correspond to the spaces between the spherical aggregates of the horn structures, and these pores would be eliminated by further re-aggregation, as shown by SEM images in Fig. 3. This re-aggregation would be caused by the bridging of acid functional groups formed on the surface of the SWCNH and ox-SWCNH by the sulfonation reaction. The micropores in the narrow spaces between the horn structures [30,31] would remain and the high surface area would be retained when re-aggregation occurs. (2) The surface area of SWCNH was doubled because small mesopores were opened by sulfonation. The opening of small mesopores by sulfonation can be considered to be similar to the mild oxidation treatment applied to produce ox-SWCNH. It has been reported that five-ring carbon structures are thermally weaker than six-ring carbon structures, and these weak sites in ox-SWCNH were already open before sulfonation [39–41]. Thus, further opening of small mesopores did not occur in ox-SWCNH upon sulfonation.

In the case of AC, the narrow pore-size distribution, as shown in Fig. 1(c), was not affected by sulfonation. As can also be seen in Table 1, the BET surface area and mesopore volume of AC were not significantly altered by sulfonation. This result leads us to consider that the acid functional group is not incorporated into the AC pores. Therefore, it is possible that the acid functional groups are located only on the outer surfaces of the AC particles. Also in the case of CB, the BET surface area and its mesopore volume did not seem to change significantly after sulfonation.

Table 2
Acid site density and TOF of solid catalysts determined by Eq. (2) for liquid-phase esterification of palmitic acid with methanol. (Reaction conditions: weight of catalyst, palmitic acid, and methanol = 0.15, 0.15, and 5 g; temperature = 64 °C; reaction time for maximum yield and TOF = 5 and 2 h respectively.).

Catalysts	Acid site density ($\mu mol\ g^{-1}$-cat)	Maximum methyl palmitate yield (%)	TOF (min^{-1})
SO_3H-SWCNHs	504	93	0.11
SO_3H-ox-SWCNHs	250	50	0.08
SO_3H-CB	316	58	0.12
SO_3H-AC	182	35	0.06

3.2. Raman analysis

It is common to conduct a structural analysis of nanotube-family materials using Raman spectroscopy. Fig. 4 shows the results of the Raman analysis for the five specimens: SWCNH, SO_3H-SWCNH, SO_3H-ox-SWCNH, SO_3H-AC, and SO_3H-CB. The intensities of the peak observed at 1560 cm^{-1}, which corresponds to the graphitic structure (G-band), were compared to those at 1330 cm^{-1}, which corresponds to the disordered structure (D-band). There were no significant differences in this feature for any of the materials studied here.

3.3. Acid site density

It was reported that SO_3H functional groups can be added on catalyst surface by hydrothermal sulfonation [23,24,27]. In this work, the amount of $–SO_3H$ was evaluated directly by measuring the weight-based acid site density assuming that all acid sites formed by sulfonation were $–SO_3H$ and were accessible. The results obtained from the ion-exchange titration method are shown in Table 2. It is noted that SO_3H-SWCNH had a significantly larger acid site density than SO_3H-ox-SWCNH, although the BET surface area of SO_3H-ox-SWCNH was about twice as large as that of SO_3H-SWCNH; the acid site density of SO_3H-SWCNH was twice that of SO_3H-ox-SWCNH, which is the opposite of the surface-area trend.

These results suggest that the oxidation pretreatment to increase the surface area of SWCNH inhibited sulfonation on its surface. Sulfonation caused an increase in the BET surface area of SWCNH by opening small pores, similarly to oxidation. Considering this analogy to oxidation, sulfonation would preferably occur on the weak sites of the carbonaceous structures, of which the ox-SWCNHs should have less because they were already consumed by the oxidation treatment. Therefore, the density of the viable sites for sulfonation in ox-SWCNH will be smaller than that in SWCNH, and thus, the resultant acid site density in ox-SWCNH will be smaller than that in SWCNH.

Comparing the sulfonated catalysts prepared in this study, the acid site density decreased in the following order: SO_3H-SWCNH > SO_3H-CB > SO_3H-ox-SWCNH > SO_3H-AC, suggesting that SWCNH is the best of these materials for the preparation of the catalyst. AC has fewer weak sites in its structure so that the pore structure was not changed by sulfonation, as described above. This means that AC will be the least reactive after sulfonation.

3.4. Catalytic activities for the esterification of palmitic acid

The catalytic activities of SO_3H-SWCNH, SO_3H-ox-SWCNH, SO_3H-AC, SO_3H-CB, and the homogeneous sulfuric acid catalyst were investigated by the esterification of palmitic acid with methanol. The results of the esterification in terms of the yield of methyl palmitate as a function of the reaction time are shown in Fig. 5. The values of the maximum yield obtained by the solid

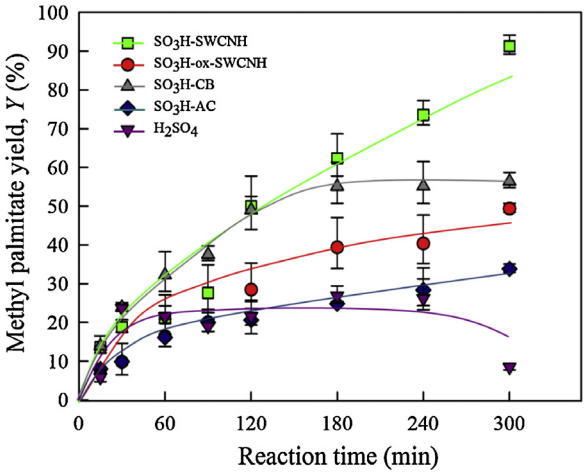

Fig. 5. Methyl palmitate yield obtained by esterification of palmitic acid with methanol (palmitic acid/methanol = 1:33) for 5 h at 64 °C catalyzed by four solid catalysts and a sulfuric acid homogeneous catalyst.

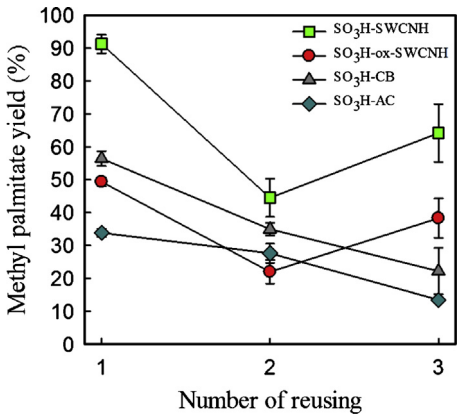

Fig. 6. Reuseability of four solid catalysts for repeated batches of esterification of palmitic acid with methanol. (Reaction conditions: weight of catalyst, palmitic acid, and methanol = 0.15, 0.15, and 5 g; temperature = 64 °C; reaction time to obtain yield in each batch = 5 h.)

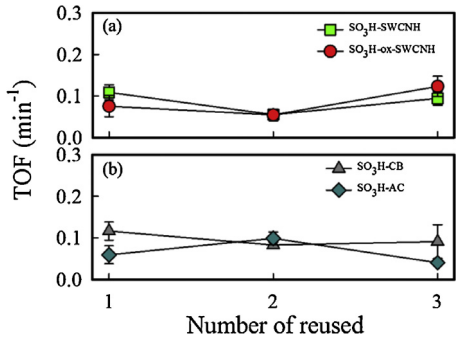

Fig. 7. Reuseability of (a) SO_3H-SWCNH and SO_3H-ox-SWCNH and (b) SO_3H-CB and SO_3H-AC for the esterification of palmitic acid with methanol. (Reaction conditions: weight of catalyst, palmitic acid, and methanol = 0.15, 0.15, 5 g; temperature = 64 °C; reaction time to obtain TOF = 2 h.)

catalysts within 5 h are shown in Table 2. It can be clearly seen that SO_3H-SWCNH has the highest catalytic performance. Based on the yield, the catalytic activities of the solid catalysts were in the order SO_3H-SWCNH > SO_3H-CB > SO_3H-ox-SWCNHs > SO_3H-AC. The yield obtained using the homogeneous sulfuric acid catalyst was almost the same as that using SO_3H-AC.

The TOFs of these solid catalysts are shown in Table 2. It should be noted that the TOFs of SO_3H-SWCNH, SO_3-ox-SWCNH, and SO_3H-CB are similar given the experimental error of ±0.02. The TOF of SO_3H-AC was lower relative to the others. Similarly to the idea of TOF, the catalytic activity of the homogeneous sulfuric acid catalyst can be evaluated from the number of moles of methyl palmitate produced per unit mole of protons from H_2SO_4 used in the esterification reaction. This value was calculated to be 0.0031. Compared with this value, the TOFs of the all of the solid catalysts prepared here are significantly higher.

It has been reported that hydrophobicity around the acid sites is an important factor for achieving high catalytic reactivity [18]. Thus, the acid sites located on the hydrophobic carbonaceous surfaces should play a critical role in the high TOF of the solid catalysts prepared in this work. As seen in Eq. (1), H_2O is formed in the esterification reaction. H_2O is known to deactivate sulfuric acid acting as a catalyst in the esterification of acetic acid with methanol by forming a strong hydration shell around the protons [42], thus hindering the access of acetic acid molecules to the sulfuric acid. As the palmitic acid is a kind of carboxylic acid, a similar phenomenon could occur. Therefore, it is expected that inhibiting hydration around the acid sites using carbonaceous support materials should significantly enhance catalytic reactivity in the esterification of palmitic acid.

To summarize the acid site density and TOF results, SO_3H-SWCNH has a high acid density and high TOF, and thus, exhibits the highest catalytic activity for the esterification of palmitic acid. The results shown in Fig. 5 reflect these conclusions.

3.5. Catalyst reusability

One of the main advantages of heterogeneous solid catalysts over liquid catalysts is that solid catalysts can be easily recovered from the reaction mixture so that they can be regenerated for reuse. In the present study, the catalytic reusability was examined by recovering the catalysts used after 5 h of reaction time. Fig. 6 shows the results for three successive batches of the esterification of palmitic acid. In this figure, activity loss can be seen for all catalysts.

Nevertheless, the TOF of these catalysts was not reduced by repeated use, as shown in Fig. 7, meaning that the active sites were not deactivated by repeated use. Hence, it is thought that the number of acid sites was reduced by repeated use. As shown in Fig. 6, the yield loss continued over three batches when SO_3H-AC and SO_3H-CB were used. In contrast, yield loss was observed only in the second batch in the case of SO_3H-SWCNH and SO_3H-ox-SWCNHs. The stability of the acid sites on SWCNH observed in this experiment also suggests that SO_3H-SWCNH is the preferable catalyst for the esterification of palmitic acid.

4. Conclusions

Four solid catalysts, SO_3H-SWCNH, SO_3H-ox-SWCNH, SO_3H-AC, and SO_3H-CB, were prepared by hydrothermal sulfonation. It was found that sulfonation reduced the number of pores larger than 20 nm in SWCNH and ox-SWCNH, and increased the BET surface area of SWCNH by a factor of two. These structural changes were not observed for AC and CB. The acid site densities present in these catalysts were analyzed by ion-exchange titration, and it was found that SO_3H-SWCNH had the highest acid site density. The intrinsic activities of the catalysts were investigated by liquid-phase esterification of palmitic acid with methanol to produce methyl palmitate. Based on the yield, SO_3H-SWCNH showed the highest reactivity. In addition, this reactivity was significantly higher than that of the homogeneous sulfuric acid catalyst. Repeated esterification experiments suggested that the acid sites on SO_3H-SWCNH and SO_3H-ox-SWCNH were more stable than those on AC and CB.

From the results of this study, it is proposed that SO_3H-SWCNH is a suitable catalyst for the production of methyl palmitate by the esterification of palmitic acid owing to the high acid site density and high TOF on its hydrophobic surface.

Acknowledgement

This work was financially supported by a JSPS Postdoctoral Fellowship for Foreign Researchers FY 2012.

References

[1] V.B. Borugadda, V.V. Goud, Renew. Sustain. Energy Rev. 16 (2012) 4763–4784.
[2] A. Talebian-Kiakalaieh, N.A.S. Amin, H. Mazaheri, Appl. Energy 104 (2013) 683–710.
[3] T. Hayashi, H. Habaki, R. Egashira, J. Chem. Eng. Jpn. (2013), http://dx.doi.org/10.1252/jcej.12we285.
[4] A.P.S. Chouhan, A.K. Sarma, Renew. Sustain. Energy Rev. 15 (2011) 4378–4399.
[5] Q. Shu, J. Gao, Z. Nawaz, Y. Liao, D. Wang, J. Wang, Appl. Energy 87 (2010) 2589–2596.
[6] I.M. Atadashi, M.K. Aroua, A.R. Abdul Aziz, N.M.N. Sulaiman, J. Ind. Eng. Chem. 19 (2013) 14–26.
[7] J.M. Marchetti, V.U. Miguel, A.F. Errazu, Renew. Sustain. Energy Rev. 11 (2007) 1300–1311.
[8] A. Islam, Y.H. Taufiq-Yap, C.M. Chu, E.S. Chan, P. Ravindra, Process Saf. Environ. Prot. 91 (2013) 131–144.
[9] M. Kouzu, A. Nakagaito, J.S. Hidaka, Appl. Catal. A 405 (2011) 36–44.
[10] S.Z. Abidin, K.F. Haigh, B. Saha, Ind. Eng. Chem. Res. 15 (2012) 14653–14664.
[11] O. Babajide, N. Musyoka, L. Petrik, F. Ameer, Catal. Today 190 (2012) 54–60.
[12] M.N. Siddiquee, H. Kazemian, S. Rohani, Chem. Eng. Technol. 34 (2011) 1983–1988.
[13] A. Patel, V. Brahmkhatri, N. Singh, Renew. Energy 51 (2013) 227–233.
[14] N. Laosiripojana, W. Kiatkittipong, W. Sutthisripok, S. Assabumrungrat, Bioresour. Technol. 101 (2010) 8416–8423.
[15] A.A. Kiss, A.C. Dimian, G. Rothenberg, Adv. Synth. Catal. 348 (2006) 75–81.
[16] L. Xu, Y. Wang, X. Yang, X. Yu, Y. Guo, J.H. Clark, Green Chem. 10 (2008) 746–755.
[17] M.A. Harmeer, Q. Sun, Appl. Catal. A 221 (2001) 45–62.
[18] T. Okuhara, Chem. Rev. 102 (2002) 3641–3666.
[19] G.D. Yudav, J.J. Nair, Microporous Mesoporous Mater. 33 (1999) 1–48.
[20] R. Lui, X. Wang, X. Zhao, P. Feng, Carbon 46 (2008) 1664–1669.
[21] A.M. Puziy, O.I. Paddubnaya, Y.N. Kochkin, N.V. Vlasenko, M.M. Tsyba, Carbon 48 (2010) 706–713.
[22] M. Toda, A. Takagaki, M. Okamura, J.N. Kondo, S. Hayashi, K. Domen, et al., Nature 438 (2005) 178.
[23] L. Roldan, I. Santos, S. Armenise, J.M. Fraile, E. Garcia-Bordeje, Carbon 50 (2012) 1363–1372.
[24] Q. Shu, Q. Zhang, G. Xu, Z. Nawaz, D. Wang, J. Wang, Fuel Process. Technol. 90 (2009) 1002–1008.
[25] Q. Shu, Q. Zhang, G. Xu, J. Wang, Food Bioprod. Process. 87 (2009) 164–170.
[26] J.A. Sanchez, D.L. Hernandez, J.A. Moreno, F. Mondragon, J.J. Fernandez, Appl. Catal. A 405 (2011) 55–60.
[27] Q. Li, S. Chen, L. Zhuang, X. Xu, H. Li, J. Mater. Res. 27 (2012) 3083–3089.
[28] R. Yuge, T. Manako, K. Nakahara, M. Yasui, S. Iwasa, T. Yoshitake, Carbon 50 (2012) 5569–5573.
[29] S. Bandow, F. Kokai, K. Takahashi, M. Yudasaka, L.C. Qin, S. Iijima, Chem. Phys. Lett. 321 (2000) 514–519.
[30] K. Murata, K. Kaneko, F. Kokai, K. Takahashi, M. Yudasaka, S. Iijima, Chem. Phys. Lett. 331 (2000) 14–20.
[31] K. Murata, J. Miyawaki, M. Yudasaka, S. Iijima, K. Kaneko, Carbon 43 (2005) 2826–2830.
[32] M. Boaventura, L. Brandao, A. Mendes, J. Electrochem. Soc. 158 (2011) B394–B401.
[33] L. Brandao, C. Passeira, D.M. Gattia, A. Mendes, J. Mater. Sci. 46 (2011) 7198–7205.
[34] Y. Lui, C.M. Brown, D.A. Neumann, D.B. Geohegan, A.A. Puretzky, C.M. Rouleau, et al., Carbon 50 (2012) 4953–4964.
[35] J. Xu, M. Yudasaka, S. Kouraba, M. Sekido, Y. Yamamoto, S. Iijima, Chem. Phys. Lett. 461 (2008) 189–192.
[36] N. Sano, J. Phys. D: Appl. Phys. 37 (2004) L17–L20.
[37] N. Sano, T. Suzuki, K. Hirano, Y. Akita, H. Tamon, Plasma Sources Sci. Technol. 20 (2011) 034002.
[38] E.P. Barrett, L.G. Joyner, P.P. Halenda, J. Am. Chem. Soc. 73 (1951) 373–380.
[39] S. Utsumi, J. Miyawaki, H. Tanaka, Y. Hattori, T. Itoi, N. Ichikuni, et al., J. Phys. Chem. B 109 (2005) 14319–14324.
[40] N. Sano, Y. Akita, H. Tamon, J. Appl. Phys. 109 (2011) 124305.
[41] G. Chen, Q. Peng, H. Mizuseki, Y. Kawazoe, Comput. Mater. Sci. 49 (2010) S378–S382.
[42] Y. Lui, E. Lotero, J.G. Goodwin Jr., J. Mol. Catal. A: Chem. 245 (2006) 132–140.
[43] X. Mo, D.E. López, K. Suwannakarn, Y. Liu, E. Lotero, J.G. Goodwin Jr., C. Lu, J. Catal. 254 (2008) 332–338.